MSci Project Report

PUTTING QUANTUM INTO MECHANICS: Modelling Quantum Transport in Nanoelectromechanical Systems

2nd May 2017

CID: 00840087
PROJECT CODE: CMTH-MacKinnon-2
SUPERVISOR: Prof. Angus MacKinnon
ASSESSOR: Dr. Derek Lee
WORD COUNT: 9906

ABSTRACT

This MSci project report details the theoretical investigation of quantum transport in Nanoelectromechanical Systems (NEMS), using the mathematics of non-equilibrium Green's functions. A model of two leads coupled to a quantum dot at finite temperatures is set up, and expressions for the current across the lead-dot-lead junction and the density of electrons on the quantum dot are derived, and then computed in the Wolfram Mathematica functional programming language. A Quantum Harmonic Oscillator (QHO) is then coupled to the system, with the current and density studied once more. Novel results such as observing the thermoelectric effect on the current, and detecting entanglement in the density of the QHO-coupled system, are achieved and discussed, and provide a basis for future theoretical explorations.

DECLARATION

In this project the non-equilibrium Green's function methodology is applied to a model of a simple nano-electromagnetic system consisting of an oscillator coupled electromagnetically to a single electron transistor. The starting point for this work was a chapter of the PhD Thesis of Muhammad Tahir, which, however, only considered the zero temperature case and did not consider entanglement. The students were required to understand the methodology and extend it to finite temperature using the Matsubara sum to implement the integration over the Fermi function. I suggested this could most easily be accomplished using Mathematica, but the code required was almost entirely written by the students themselves.

In general 00731717 and 00840087 worked as a team through the whole period of the project, particularly as far as the mathematical derivations were concerned. However, 00731717 did more in the early stages, took more responsibility for the Mathematica coding and, in the later stages, did more work on entanglement.

Angus MacKinnon, 10th April 2017

ACKNOWLEDGEMENTS

My main acknowledgements go to Professor MacKinnon, who persevered in guiding my project partner and I through a topic full of obscurity; my project partner 00731717 – '007' for short – for pushing me to keep working and providing a year's worth of constructive discussions; and Muhammad Tahir, whose PhD Thesis this project is built upon.

Also, a hat-tip goes to the IT helpdesk at Imperial College for helping me and my project partner secure licenses to install Mathematica on our home machines. This allowed a lot of work to be done remotely and flexibly around other commitments.

Lastly, it is worth acknowledging the online communities on sites such as Stack Overflow, which provide a wealth of knowledge to help tackle and solve programming problems.

N.B All the programming scripts used in this report to derive results and generate graphs were self-written, despite what the end of the Declaration above implies.

CONTENTS

1 INTRODUCTION

1.1 HISTORY & INTEREST

Today's research into nanoelectromechanical systems (NEMS) can be traced back to a 1959 talk by physicist Richard Feynman, titled "There's Plenty of Room at the Bottom", where the benefits of the ability to build and coordinate 'machines' at smaller and smaller scales (up to even atom-by-atom manipulation) were proposed [1] [2]. Through the 1980s and 1990s, the production of microelectromechanical systems (MEMS) became well established, and progress since then has turned to the yet smaller scale of NEMS.

NEMS provide a particular interest as their size approaches the 'border' between what is understood to behave in a classical manner (described well by Newton's laws of motion) and the atomic world, which is best described by quantum mechanics. The fundamental purpose of probing this border is to help further the understanding of how the quantum substructures of the universe coalesce to produce the classical reality we observe at larger scales.

Not only is this question of deep importance in the philosophy of science and nature, but better understanding of how to achieve quantum behaviour at larger scales could give rise to powerful new tools and technologies (such as qubits for quantum computing [3], or magnetic resonance force microscopy for atom-resolution molecular imaging [1]) which can in turn advance all areas of science.

1.2 NANOELECTROMECHANICAL SYSTEMS (NEMS)

In general, an electromechanical system requires two parts: a mechanical component and an electrical component.

Typical choices for the mechanical component in NEMS include a cantilever (a vibrating beam suspended at one end); a bridge (a vibrating beam suspended at both ends); or a torsion balance (the rotational analogue to a spring-mass pendulum). These are popular as they are easily miniaturised, and can be made from materials already commonly processed in the computer industry, such as silicon, gallium arsenide, indium arsenide and even silicon nitride [1] [3]. More modern NEMS have been constructed using carbon-based materials such as diamond, nanotubes, or graphene [2] [4].

Secondly, the electrical component must act as a transducer. This means it must both convert the mechanical energy of the mechanical component into electrical energy, and be a conduit for electrical energy to be converted back into mechanical energy [1].

Due to this coupling, electromechanical systems become interesting examples of non-trivial dynamical systems in their own right - whatever the scale - even if explicitly quantum behaviour is not observed [5].

Figure 1A below outlines a simple example of an electromechanical system, where an oscillating charged mass is placed between an electrical tunnel junction under an applied bias.

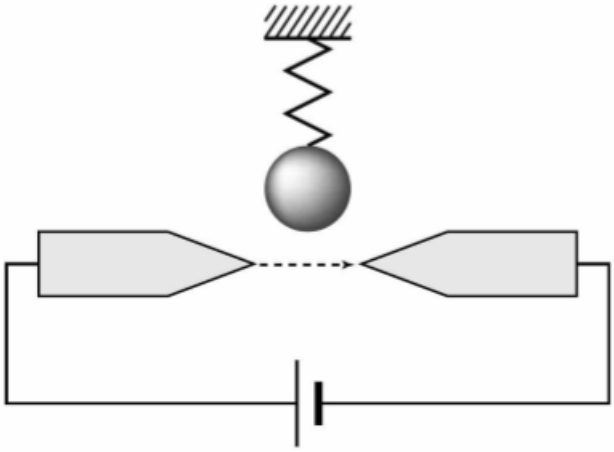

Figure 1A [5]. *A diagram depicting an example of an electromechanical system. A charged mass oscillates between two electrodes, known as an electrical tunnel junction, under an applied bias, and modulates the rate at which electrons are able to cross the junction. The current generated by this will in turn generate an electric field, which will affect the motion of the charged mass. Thus, the two components are coupled, with the strength of the coupling controllable by varying either the applied bias, or the charge on the mass.*

The oscillating position of the charged mass affects the rate at which electrons traverse the junction, and hence the current through the circuit modulates. This current in turn affects the electric field the charged mass experiences, and hence affects its oscillating motion.

In this way, the two components, electrical and mechanical, are coupled, with the strength of the coupling controlled by varying the charge on the mass, or the voltage across the circuit.

1.3 SINGLE ELECTRON TRANSISTOR (SET)

One of the most prominently used transducer mechanisms found in NEMS is the single electron transistor (SET).

A SET is comprised of an 'island' in between a source and a drain electrode, which is sufficiently small that individual electrons can quantum tunnel from drain to source due to a constant drain-source voltage. The number of electrons tunnelling through the island is then controlled by a varying bias applied across a third electrode, the gate.

Figure 1B shows a SET implemented into a NEMS.

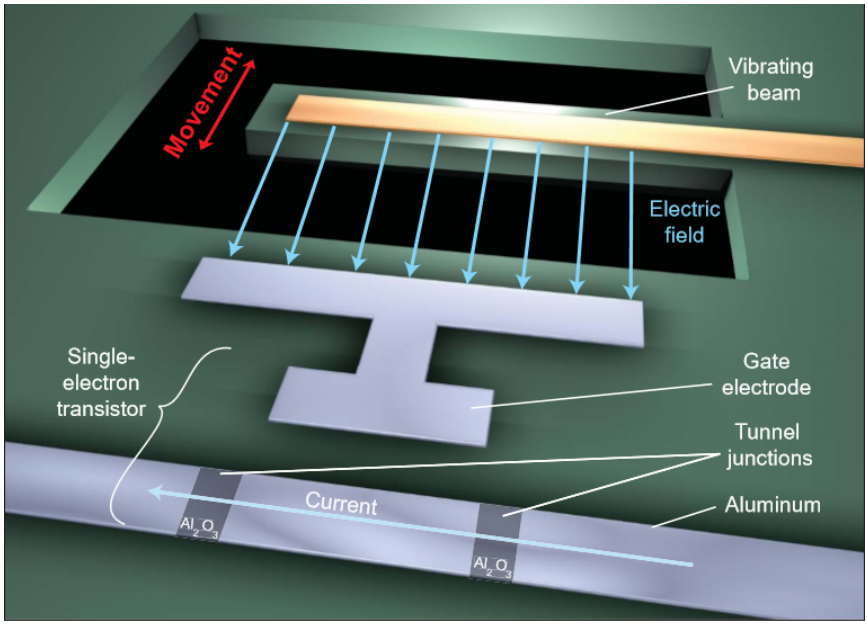

Figure 1B [3]. *A nanoelectromechanical system (NEMS) built with a vibrating beam (cantilever) coupling to a single electron transistor (SET). The beam's vibrations modulate the electric field across the transistor's gate, varying the gate's voltage and hence affecting the 'current' of individual electrons which can flow out of the system. In turn, due to the tiny effective mass of the beam, the exit of one of these electrons gives the beam a 'kick', which then modulates the electric field once more. In this way, the system couples the mechanical and electrical components at a nano-to-quantum scale, allowing for the potential probing of quantum behaviour.*

The vibration of the mechanical component (in this case, a cantilever) affects the electric field acting on the transistor, which varies the voltage across the transistor gate. This determines whether an electron is able to leave the drain. In turn, an electron leaving has a 'kick' effect on the vibration of the beam, due to the very small mass of the beam. Thus, the mechanical and electrical components are coupled, and their interaction can be measured by the current flowing from the SET.

1.4 REPORT OUTLINE

The aim of this project is to develop a theoretical understanding of NEMS by investigating a model of quantum transport across a SET-like junction. The model is built by first constructing a theoretical framework to describe the system, and then coupling this to a Quantum Harmonic Oscillator (QHO).

The conceptual structure of the model is shown in Figure 1C: two leads of given Fermi energy levels, with the junction between them connected by a quantum dot (a single energy level). This dot is in turn coupled to a QHO. This is shown diagrammatically in Figure 1C.

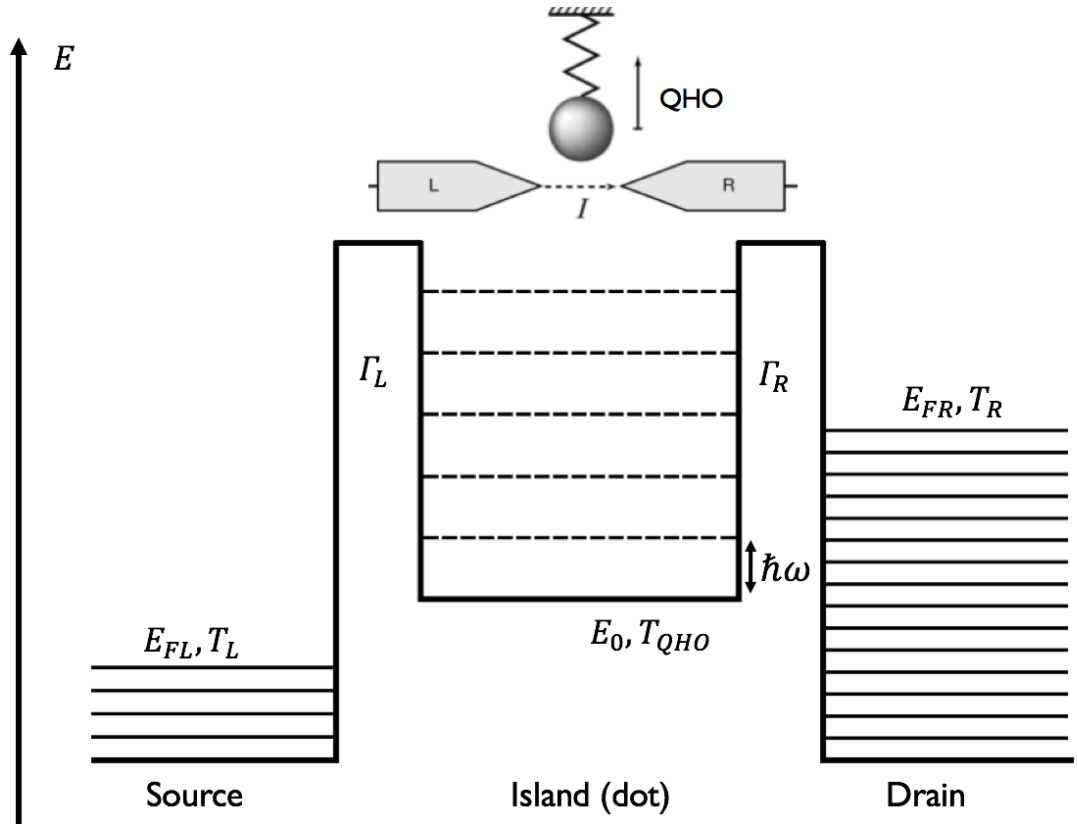

Figure 1C. A diagrammatic representation of the QHO-coupled model used in this project, suggestive of its SET-like nature. The parameters include: the Fermi energies of each lead (E_{FL}, E_{FR}); the quantum dot energy level (E_0); the temperatures of each lead and the QHO (T_L, T_R, T_{QHO}); and the tunnelling rate energies (Γ_L, Γ_R), which are introduced in Section 2.3. The solid lines represent the energy levels in the leads, and the dotted lines the QHO energy level 'ladder', separated by ħω.

The rate of electron transport[1] across this junction from one lead, to the dot, then onto the next lead determines the 'single electron' current that is of interest, amongst other properties of the system which are also investigated, such as the density of electrons on the dot.

The project's work is based upon the work of Muhammad Tahir's PhD thesis. Tahir's work was limited by an inability to derive results for a system at non-zero temperatures, due to a difficulty in integrating Fermi functions. By reformulating the Fermi function as a sum of individual terms (known as Matsubara frequencies), the integrations could be performed on the individual terms and then summed. This allowed for the derivation of definite, analytic final expressions for the model at non-zero temperatures, which is the main body of work of this project.

The mathematical basis of the model is the use of Green's functions - in particular, the use of non-equilibrium Green's functions – to describe the transport of electrons across the junction.

[1] The electron transport from lead to dot (and vice versa) is achieved via resonant tunnelling.

Non-equilibrium Green's functions act as particle propagators[2], in this case transporting electrons across the lead-dot-lead system.

Using this mathematical formalism in conjunction with perturbation theory, the Hamiltonian for the lead-dot-lead system can be constructed, and an expression for the current derived. This will be described in Section 2. [6] [7] [8] [9] [10]

The current is then investigated as a function of the dot energy. The final mathematical expression of the current is derived and computed in Mathematica, with its structure discussed in Section 3.

Then, current vs. the dot energy is plotted, and the effects on the current of varying the temperatures of each lead are shown and discussed, along with investigations of the density of electrons on the dot. The theoretical method and graphical results are described in Section 4.

The coupling of the QHO to the system is achieved by considering the overlap wavefunctions of the quantum dot in occupied and unoccupied states. The interactions with the phonons of the QHO are modelled as a scattering process. The theoretical basis for applying this to the Green's functions formalism is outlined in Section 5. [6]

Expressions for current and density are again able to be derived for this QHO coupled system, and results are obtained through numerical computations. First, the current is again studied for the QHO-coupled system. Then, the density matrix of the system is studied in terms of the quantum entanglement it exhibits. These results are shown and discussed in Section 6.

Lastly, conclusions are drawn in Section 7, and the possibility of future explorations discussed.

[2] It is from this propagation of the particles (in this case the movement of electrons) that the non-equilibrium Green's functions earn their 'not at equilibrium' status.

2 THEORETICAL BASIS

2.1 GREEN'S FUNCTIONS

The theoretical approach of this project heavily relies on the use of Green's functions as applied to condensed matter physics. In quantum mechanical terms, building a model concerned with single particle dynamics relies on the single particle Schrodinger equation:

$$\left(E_n - \widehat{H}\right)\psi_n = 0 \tag{2.1}$$

In Equation 2.1, E_n are the energy eigenvalues for the corresponding energy eigenfunctions ψ_n (which form a complete and orthonormal set of states) of the single particle Hamiltonian, $\widehat{H}$ (the energy operator). Choosing a particular Hamiltonian is the first step in describing any model of a microscopic system in condensed matter physics.

Although a more proper foundation of the use of Green's functions in quantum transport is built on quantum field theoretical arguments, for the purposes of this project the following initial definition is used:

$$\left(E - \widehat{H}\right)G(E) = 1 \tag{2.2}$$

This describes a function $G(E) = (E - \widehat{H})^{-1} = (E - E_n)^{-1}$ which is defined for all energies apart from the energy eigenvalues, E_n, of the Hamiltonian. The energies $E = E_n$ for which the Green's function is undefined are referred to as singularities. Here, E, stands for the total energy of the system, and is a continuous variable.[3]

2.2 PERTURBATION THEORY & THE SELF-ENERGY

To describe the Hamiltonian of the lead-dot-lead system, perturbation theory is used. The unperturbed system is taken to be made of the dot and leads as independent systems, before any coupling; the perturbation is taken as the coupling of the leads to the dot. The overall Hamiltonian for the dot is then:

$$\widehat{H} = H_0 + dH \tag{2.3}$$

[3] It is noted that the Green's function is defined as function of energy (effectively, in frequency space). This is as opposed to being defined as a function of time (in momentum, or wavevector k-space), as is more common in quantum field theories. As this project's investigation is into the behaviour of a system once it reaches a final steady state (in, say, its current or density), it is then possible for the Green's functions used to be functions of energy, Fourier transformed from being functions of time.

where H_0 corresponds to the Hamiltonian of the uncoupled dot (with energy eigenvalue E_0), and dH corresponds to the perturbation of the coupling.

Mathematically, the unperturbed Green's function $g(E)$ is defined as:

$$g(E) = (E - H_0)^{-1} = (E - E_0)^{-1} \tag{2.4}$$

where E is the total energy, and E_0 is the unperturbed energy level of the dot (the eigenvalue of H_0).

The perturbed, full Green's function $G(E)$ is defined by:

$$G(E) = \left(E - \widehat{H}\right)^{-1} = (E - H_0 - dH)^{-1} \tag{2.5}$$

From this, a reflexive form of G can be derived involving the unperturbed g:

$$(E - H_0 - dH)G = 1$$

$$(E - H_0)G = 1 + dH \cdot G$$

$$G = (E - H_0)^{-1} \cdot (1 + dH \cdot G) = g(1 + dH \cdot G)$$

$$G = g + g \cdot dH \cdot G \tag{2.6}$$

This way of writing the perturbed G (as a function of the unperturbed g and itself) is known as the standard Dyson's equation with single particle perturbation, and is important in its use in quantum field theories.

The energy eigenvalue of the perturbation term in the overall Hamiltonian is known as the self-energy, written with a capital sigma Σ. The self-energy represents the exact change to the dot energy level due to its coupling with the leads. Substituting Σ for dH and E_0 for H_0 into equation 2.5 above, the final form of the perturbed Green's function can be written:

$$G(E) = (E - E_0 - \Sigma)^{-1} \tag{2.7}$$

2.3 ADVANCED & RETARDED GREEN'S FUNCTIONS

In Green's functions theory, two types of function can be distinguished by the time order in which they apply. An advanced function, written G^a, is defined by being non-zero only before a perturbation occurs. A retarded Green's function, written G^r, is defined by being non-zero only after the perturbation.

These Green's functions can be written in the same form as in equation 2.7 above, where the difference between the advanced and retarded forms is due to the self-energy term being designated as either advanced (Σ^a), or retarded (Σ^r).

The retarded and advanced Green's functions are thus written:

$$G^{a(r)} = (E - E_0 - \Sigma^{a(r)})^{-1} \tag{2.8}$$

In order to calculate the self-energies, an assumption needs to be made that the contributions to the dot energy from each lead (labelled $\alpha = L, R$ for the left and right leads respectively) are independent of each other. This is known as the wide-band approximation. The self-energies from each lead can then be calculated via an integral over the energy states of the leads. The result is:

$$\Sigma_\alpha^a = (\Sigma_\alpha^r)^* = \frac{i\Gamma_\alpha}{2} \tag{2.9}$$

In equation 2.9, capital gamma Γ_α is a lead-dependent energy scale determined by the density of states (n_α) in the lead, and the potential barrier between the dot and that lead V_α (also known as the hopping potential).[4] Ultimately, the value of the energy Γ_α represents how much resonant tunnelling can occur, and is thus called the tunnelling rate energy in this report.

The imaginary nature of the self-energies arises because the integration of the energy states of the leads is performed in the complex plane. This is necessary to account for singularities which occur in the Green's functions.

The complex conjugation relationship between the retarded and advanced self-energies is fundamentally due to their time ordering difference, and can be thought of as a minus sign entering the calculation due to a swapping of limits on the integral.

It is worth noting, for completeness, that:

$$\Sigma^{a(r)} = \Sigma_L^{a(r)} + \Sigma_R^{a(r)} \tag{2.10}$$

In which case, it is useful to define the following 'average gamma':

$$\bar{\Gamma} = \frac{1}{2}(\Gamma_L + \Gamma_R) \tag{2.11}$$

Such that then:

$$(\Sigma^r)^* = \Sigma^a = i\bar{\Gamma} \tag{2.12}$$

[4] Specifically, $\Gamma_\alpha = 2\pi \cdot n_\alpha \cdot |V_\alpha|^2$

2.4 NON-EQUILIBRIUM GREEN'S FUNCTIONS

The non-equilibrium Green's function that is used in this project is $G^<$ (said "G lesser"), defined by:

$$G^< = f \cdot (G^a - G^r) \tag{2.13}$$

where f is the Fermi function of the system. The Fermi function describes the distribution of electrons in the energy levels of a material at different temperatures. The Fermi energy is the energy at which, at the absolute zero of temperature, all energy levels below are filled with electrons, and all energy levels above are empty. [11]

For the lead-dot-lead model, the Fermi function is where the information on the electrons in the leads is introduced. Since there are two leads (left and right), the contributions from both individual Fermi functions need to be considered.

The Fermi functions for the individual leads is given by:

$$f_\alpha = \frac{1}{1 + e^{(E - E_{F\alpha})/k_B T_\alpha}} \tag{2.14}$$

where E is the total energy of the system; $E_{F\alpha}$ is the Fermi energy of the left or right leads ($\alpha = L, R$); k_B is Boltzmann's constant; and T_α is the temperature of each lead.

In order, then, to account for the Fermi functions of both leads, f in equation 2.13 is taken as a weighted average[5] of the two f_α, with the weights given by the tunnelling rates for each lead, Γ_α:

$$f = \frac{\Gamma_L f_L + \Gamma_R f_R}{\Gamma_L + \Gamma_R} \tag{2.15}$$

Equation 2.13 is an example of the more general formula for 'lesser' functions applied to the Green's function. Written in words for clarity, this general formula is:

$$Lesser = Fermi * (Advanced - Retarded) \tag{2.16}$$

This can be applied to the self-energies in each lead, giving the following expression for the lesser self-energy of each lead:

$$\Sigma_\alpha^< = f_\alpha(\Sigma_\alpha^a - \Sigma_\alpha^r) = f_\alpha\left(\frac{i\Gamma_\alpha}{2} - \frac{-i\Gamma_\alpha}{2}\right)$$

$$\Sigma_\alpha^< = i f_\alpha \Gamma_\alpha \tag{2.17}$$

[5] As the Fermi function is simply a probability distribution for the energy states of the electron, it makes intuitive sense to take the statistical expected value (the weighted average) when needing to combine two together.

Combining equations 2.17 with 2.13, it can be shown that $G^<$ may be rewritten as:

$$G^< = G^r \Sigma^< G^a \tag{2.18}$$

2.5 THE CURRENT EQUATION

To derive the equation for the single electron current across the lead-dot-lead system, two results are used.

The first is the core relation to quantum mechanics of the non-equilibrium Green's functions technique:

$$\rho = \frac{1}{2\pi i} \int_{-\infty}^{\infty} G^< \, dE \tag{2.19}$$

where ρ is, in general, the density matrix of the energy states of the system. In the case of the lead-dot-lead system, this density matrix is a 1×1 matrix, as there is only one state of interest (the energy eigenstate on the dot). This value can be interpreted as the likelihood of an electron being detected in the dot's energy level.

The second result used is that of $\hat{I}_\alpha$, the operator for the particle current (the flow of electrons between each lead and the dot):

$$\hat{I}_\alpha \, / \frac{e}{\hbar} = \, i \sum_j V_\alpha (c_0^\dagger c_{\alpha,j} - c_{j,\alpha}^\dagger c_0) \tag{2.20}$$

In equation 2.20, e is the elementary charge; $\hbar$ is the reduced Planck's constant; V_α is the hopping potential from each lead to the dot (and vice versa); $c_0^\dagger$ and c_0 are, respectively, the creation and annihilation operators for electrons on the dot; and lastly, $c_{j,\alpha}^\dagger$ and $c_{\alpha,j}$ are, respectively, the creation and annihilation operators for electrons at the j^{th} energy level of each lead.

As is suggested by its constituents, this operator tells us explicitly about the creation and annihilation of electrons on the dot and the leads. If the creation of electrons on dot and annihilation of electrons on leads perfectly equals the creation in the leads and annihilation on the dot, then there is no overall electron flow from dot to lead (or vice versa). Any imbalance however, results in a finite current.

It is noted that this operator is determined in units of $e/\hbar$, the natural unit for particle current in quantum mechanics.[6] These units will be omitted in future derivations and results. This

[6] In SI units, $[e/\hbar] = \, A \cdot s^2 \cdot kg^{-1} \cdot m^{-2}$.

omission can be interpreted as the use of natural units, often favoured in theoretical physics, where $e = \hbar = 1$ and are dimensionless.

Combining 2.19 and 2.20, the expected value I_α of the current operator can be found using the relation:

$$I_\alpha = Tr(\rho \hat{I}_\alpha) \tag{2.21}$$

As the eigenstates and eigenvalues of the current operator are continuous, this trace turns into an integration over the total energy of the system.

Ultimately, the following result for the current from each lead can be derived:

$$I_\alpha = \frac{1}{2\pi} \int_{-\infty}^{\infty} \Sigma_\alpha^< (G^r - G^a) + G^< (\Sigma_\alpha^a - \Sigma_\alpha^r) dE \tag{2.22}$$

Note that this is a value representing the flow of electrons as quantum particles from one lead to the dot, meaning it is always a positive value. The single electron current (the quantum mechanical electrical current), is then taken as the difference between the contributions of left and right leads:[7]

$$I = I_L - I_R \tag{2.23}$$

From this, the single electron current can be written:

$$I = \frac{1}{2\pi} \int_{-\infty}^{\infty} (\Sigma_L^< - \Sigma_R^<)(G^r - G^a) dE - (\Gamma_L - \Gamma_R)\rho \tag{2.24}$$

This form of the current equation highlights a core physical concept: any difference in the tunnelling rate energies allows for a contribution to the current directly due to the density of electrons on the dot. This source of current can be interpreted as electron density 'leaking' from dot to lead through the tunnelling barrier with the higher tunnelling rate.

2.6 THE MATSUBARA SUM

To model the desired system using equation 2.24, the energy integral of the Fermi function (coming into the integration via the lesser self-energies) must be computed. In its normal form (equation 2.14) this integral does not converge. In his PhD, Muhammad Tahir resolved this by limiting the temperature to absolute zero, wherein the Fermi function becomes a Heaviside step function. The integrals were thus made possible.

[7] It is also worth noting that, by writing the current as $I_L - I_R$, as opposed to $I_R - I_L$, the particle flow from the left to right is defined as the positive direction.

In this project however, to retain a non-zero temperature in the model, the Fermi function is rewritten in the following way:

$$f_\alpha = \frac{1}{2} - \sum_{q=-\infty}^{\infty} \left\{ \frac{E - E_{F\alpha}}{k_B T_\alpha} - i(2q+1)\pi \right\}^{-1} \tag{2.25}$$

where q is the Matsubara frequency index, and all other symbols retain their meanings. The sum is known as a Matsubara sum. The imaginary components of the summation terms are known as Matsubara frequencies. [7]

For theoretical work, the following form will be used for simplicity:

$$f_\alpha = \frac{1}{2} - \sum_{q=-\infty}^{\infty} M_\alpha \tag{2.26}$$

where

$$M_\alpha = \left\{ \frac{E - E_{F\alpha}}{k_B T_\alpha} - i(2q+1)\pi \right\}^{-1} \tag{2.27}$$

Using this mathematical rewriting of the Fermi function, the energy integration can now be done on the M_α terms over the complex plane, and the final sum converges. This allows for a definite, computable, final expression for the lead-dot-lead single electron current at non-zero temperatures.

3 METHOD

3.1 COMPUTATIONAL METHOD

The computational method in this project was the use of the functional programming language and software Wolfram Mathematica.

Numerous scripts were written as calculation aids in evaluating the expressions derived using the theory. The `Integral[]` and `Sum[]` functions were used to perform the energy integrals and sums over Matsubara frequencies of the equations for current and density.

Mostly, the expressions simply needed to be transcribed from paper into the programming script. However, the key to calculating the desired results for the model was in instructing what assumptions the programme should make for each variable used. Otherwise, the variables are assumed to be general complex numbers, which does not produce physical results.

For example, the energies needed to be defined as real numbers, the temperatures as positive real numbers, and the index for labelling the Matsubara frequencies as an integer.

To ensure the `Sum[]` method performed the sum over all the required Matsubara frequencies, it was necessary to rewrite

$$\sum_{q=-\infty}^{\infty} M_\alpha = \sum_{q=0}^{\infty} M_\alpha + \sum_{-(q+1)=0}^{\infty} M_\alpha \tag{3.1}$$

and thus assume the index q to be both an integer and non-negative.

The graphs in this report were also produced using Mathematica scripts, all from analytically derived results of the model. The standard `Plot[]` function was used for this, usually nested into the `Manipulate[]` function in order for the numerous parameters in the model to be varied as the graphs plotted in real-time.

The main difference in the method of compution of the model once the QHO was coupled was in the use of functions to create matrices (`Table[]`) and mathematically manipulate them (such as `Total[]`, `Eigensystem[]`, `MatrixLog[]` and others).

3.2 SOLVING THE CURRENT EQUATION

The first result achieved in this project was the full derivation of an analytic form for the general single particle current in the lead-dot-lead model. To outline the theoretical method undertaken in this project, this derivation will be shown in detail. Other theoretical results achieved were derived in a similar fashion.

As described in Section 3.1, the work of evaluating integrals and sums was done computationally using Mathematica. This meant that the theoretical derivations focussed on writing the equations for the model in a form where all the inputs were physical properties of interest to the model. This includes either Fermi energies ($E_{F\alpha}$), temperatures of (T_α), and tunnelling rate energies (Γ_α) of each lead.

To start, equation 2.24 is restated with the density ρ rewritten as the energy integral of $G^<$:

$$I = \frac{1}{2\pi}\int_{-\infty}^{\infty}(\Sigma_L^< - \Sigma_R^<)(G^r - G^a) + i(\Gamma_L - \Gamma_R)G^< dE \tag{3.2}$$

By recalling equation 2.18, $G^<$ can be written:

$$G^< = G^r\Sigma^< G^a = G^r(\Sigma_L^< + \Sigma_R^<)G^a \tag{3.3}$$

The current equation then becomes:

$$I = \frac{1}{2\pi}\int_{-\infty}^{\infty}(\Sigma_L^< - \Sigma_R^<)(G^r - G^a) + i(\Gamma_L - \Gamma_R)(\Sigma_L^< + \Sigma_R^<)G^r G^a dE \tag{3.4}$$

Both the difference and the sum of the left and right lesser self-energies appear here. By recalling equations 2.17 and 2.25, both the sum and the difference in lesser self-energies can be written:

$$\Sigma_L^< \pm \Sigma_R^< = if_L\Gamma_L \pm if_R\Gamma_R$$

$$\Sigma_L^< \pm \Sigma_R^< = i\left(\frac{1}{2} - \sum_{q=-\infty}^{\infty} M_L\right)\Gamma_L \pm i\left(\frac{1}{2} - \sum_{q=-\infty}^{\infty} M_R\right)\Gamma_R$$

$$\Sigma_L^< \pm \Sigma_R^< = i\left(\frac{1}{2}(\Gamma_L \pm \Gamma_R) - \sum_{q=-\infty}^{\infty}\Gamma_L M_L \pm \Gamma_R M_R\right) \tag{3.5}$$

There also appears in the equation 3.4 the difference and product of the advanced and retarded Green's functions.

Recalling the results in equations 2.8 and 2.12, the advanced and retarded Green's functions can be written:

$$(G^r)^* = G^a = (E - E_0 - i\bar{\Gamma})^{-1} \tag{3.6}$$

Therefore, using the identities

$$\frac{1}{a+ib}\times\frac{1}{a-ib}=\frac{1}{a^2+b^2}$$

$$\frac{1}{a+ib}-\frac{1}{a-ib}=\frac{-2ib}{a^2+b^2}$$

the difference and the product of the two Green's functions can be derived, with $a=E-E_0$ and $b=\bar{\Gamma}$:

$$G^r-G^a=\frac{-2i\bar{\Gamma}}{(E-E_0)^2+\bar{\Gamma}^2}=\frac{-i(\Gamma_L+\Gamma_R)}{(E-E_0)^2+\bar{\Gamma}^2} \tag{3.7}$$

$$G^rG^a=\frac{1}{(E-E_0)^2+\bar{\Gamma}^2} \tag{3.8}$$

These results (equations 3.5, 3.7 and 3.8) can be plugged back in the equation 3.4, giving:

$$I=\frac{1}{2\pi}\int_{-\infty}^{\infty} i\left(\frac{1}{2}(\Gamma_L-\Gamma_R)-\sum_{q=-\infty}^{\infty}\Gamma_L M_L-\Gamma_R M_R\right)\left(\frac{-i(\Gamma_L+\Gamma_R)}{(E-E_0)^2+\bar{\Gamma}^2}\right)$$

$$+i(\Gamma_L-\Gamma_R)\cdot\, i\left(\frac{1}{2}(\Gamma_L+\Gamma_R)-\sum_{q=-\infty}^{\infty}\Gamma_L M_L+\Gamma_R M_R\right)\left(\frac{1}{(E-E_0)^2+\bar{\Gamma}^2}\right)dE \tag{3.9}$$

By noting the i's in each part of the integrand cancel, the 'difference of two squares' brackets in each part – $(\Gamma_L+\Gamma_R)(\Gamma_L-\Gamma_R)$ – also cancel, leaving:

$$I=\frac{1}{2\pi}\int_{-\infty}^{\infty}\frac{\left\{-(\Gamma_L+\Gamma_R)\sum_q\Gamma_L M_L-\Gamma_R M_R\right\}-\left\{-(\Gamma_L-\Gamma_R)\sum_q\Gamma_L M_L+\Gamma_R M_R\right\}}{(E-E_0)^2+\bar{\Gamma}^2}dE \tag{3.10}$$

Thus, by expanding out the brackets, the combinations ${\Gamma_\alpha}^2 M_\alpha$ cancel, leaving only the $\Gamma_L\Gamma_R M_\alpha$ terms. This ultimately gives the result:

$$I=\frac{1}{2\pi}\sum_{q=-\infty}^{\infty}\int_{-\infty}^{\infty}\frac{2\Gamma_L\Gamma_R}{(E-E_0)^2+\bar{\Gamma}^2}(M_R-M_L)\,dE \tag{3.11}$$

This is deliberately rewritten with the sum over Matsubara frequencies before the energy integral, as this is the order in which the computation is done for the calculation to converge.

It is noted that this expression depends solely on the variables we are interested in manipulating: the quantum dot energy E_0; each lead's tunnelling rates Γ_α; and, in the Matsubara terms M_α (equation 2.27) the Fermi levels and temperatures ($E_{F\alpha}$, T_α) for each lead.

Performing this evaluation in Mathematica, the result is:

$$I = \frac{1}{2\pi} \cdot \frac{\Gamma_L \Gamma_R}{\bar{\Gamma}} \cdot i\{\Delta\psi(z_L) - \Delta\psi(z_R)\} \tag{3.12}$$

In equation 3.12, the $\psi(z)$ is the Digamma function, defined as the logarithmic derivative of the Gamma function (the extension of the factorial operation to complex numbers).

In this result, $\Delta\psi$ denotes the difference between two Digamma functions whose arguments are complex conjugates:

$$\Delta\psi(z_\alpha) = \psi(z_\alpha) - \psi(z_\alpha^*) \tag{3.13}$$

The argument of the Digammas, z_α, is a lead-dependent complex number:

$$z_\alpha = \frac{1}{2} + \frac{\bar{\Gamma} + i(E_{F\alpha} - E_0)}{2\pi k_B T_\alpha} \tag{3.14}$$

3.3 STRUCTURE OF THE CURRENT MODEL

By considering the parameters of the model, as they appear in equation 3.12, it can be seen that their combinations make physical sense.

The arguments of the Digamma functions depend on the differences, not the absolute values, in the energy levels inputted (as required for a fundamental theory). The argument also depends on the ratio of the different energy scales: the average tunnelling rate energy and the gap between the dot and Fermi energies both appear as fractions of the overall thermal energy.

Also, the combination of the tunnelling rate energies appearing as a factor outside the more complicated Digamma functions in equation 3.12 makes sense as, fundamentally, if the amount of tunnelling changes, there will be an effect on the current, regardless of other variables.

It is worth noting that the form of how the tunnelling rate energies combine at the start of the expression can be rewritten as the reciprocal of the sum of each reciprocal:[8]

$$\frac{\Gamma_L \Gamma_R}{\bar{\Gamma}} \propto \left(\frac{1}{\Gamma_L} + \frac{1}{\Gamma_R}\right)^{-1} \tag{3.15}$$

This is the typical way to sum coefficients of two separate objects such that they can be treated as one object with a single coefficient. This is analogous to the way electrical resistances

[8] The proportionality constant is 2.

connected in parallel are combined, or how the reduced mass of a system of two bodies is calculated. Being combined in this way emphasises that the current in this system does not distinguish between the left and right tunnelling rate energies: it is identically affected by both.

Another notable aspect of this model is its behaviour under the exchange of left and right labels. As expected, this exchange of labels only changes the sign of the current, as it would then be flowing the (definitionally) opposite direction. All variables that change the magnitude of the current only appear symmetrically to left-right exchange, as required for the model to make physical sense.

Furthermore, the structure of the variables in the model mean that there are only two ways to generate current despite there being three pairs of variables ($\Gamma_\alpha, E_{F\alpha}, T_\alpha$) available to manipulate the system into an imbalance. While all three appear in the argument for the Digamma function, only the tunnelling rate energies appear in a form independent of the label for which lead it belongs to. This means that, if the only imbalance in the system from a difference in the tunnelling rate energy of each lead, then $\Delta\psi(z_L) = \Delta\psi(z_R)$, resulting in zero current. In other words, in this model, a 'gamma current' does not materialise.

4 RESULTS

4.1 CURRENT VS. DOT ENERGY

The lead-dot-lead model produces a current when the Fermi levels in each lead differ. The behaviour of this current can be explored by plotting it as a function of the dot energy.

In these current vs. dot energy graphs, the current is measured in units of $e/\hbar$ (which equal dimensionless unity in natural units). The dot energy (and all energies inputted into the model) is measured in arbitrary units, as all the physics in the model depends on the ratios of and differences in the energies, not on their absolute values. This means that the 'zero' of dot energy plotted does not correspond to any physical 'zero' of energy in general.

However, most of the interesting physics of the model does not lie in the exact values plotted on the axes, but rather in the shapes of the plots.

Figure 4A shows the current (blue line), and the two Fermi levels set at a constant gap (black lines). The black line on the left represents the left lead's Fermi level (E_{FL}), and the black line on ther right represents the right lead's Fermi level (E_{FR}).[9]

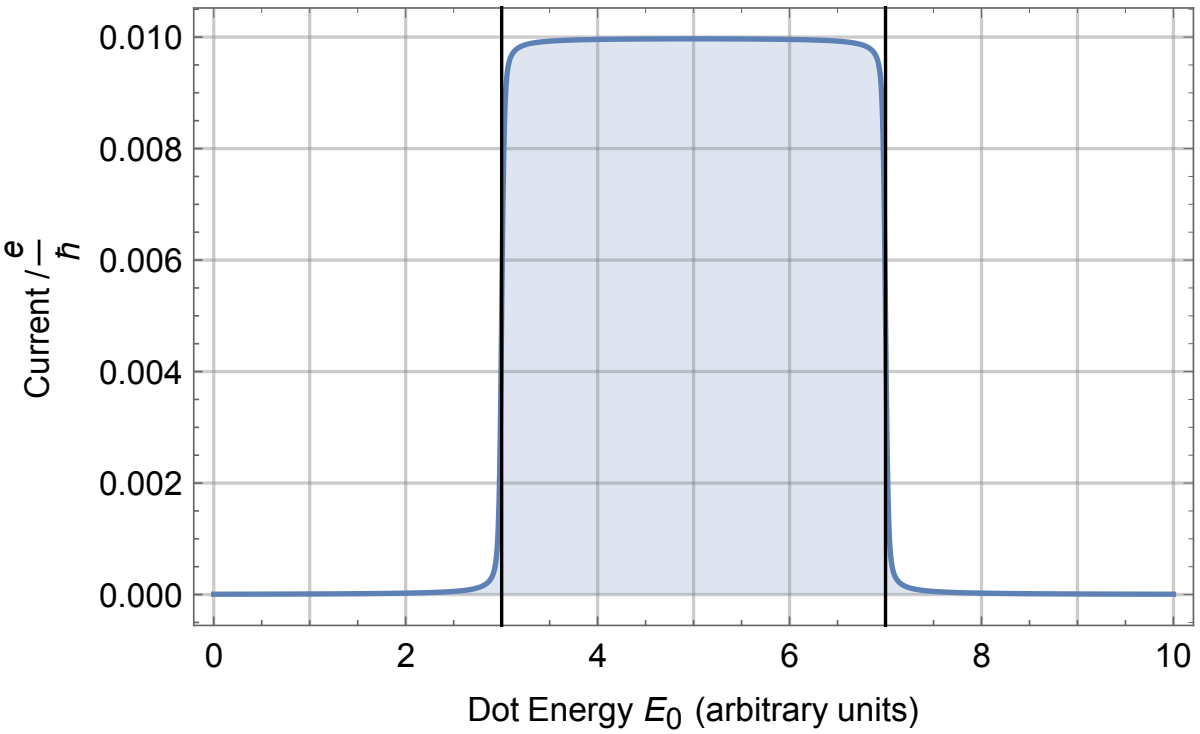

Figure 4A. A plot of current vs. dot energy in the lead-dot-lead model. The blue line indicates the current, and the black lines indicate the Fermi energies of each lead. The current begins to flow as the dot energy enters the Fermi level gap, and continues to do so throughout this region. The current then drops, eventually to zero, as the dot energy grows larger than the higher Fermi level. The slight smoothing at the transitions is due to non-zero temperatures and tunnelling rate energies.

[9] To have the left Fermi level's black line on the left of the graph, it must be defined to be lower. This would result in negative current if left-to-right is defined as the positive direction, as in Section 2.5. To be able to plot the current as greater than zero, the positive direction is defined as right-to-left for these plots.

The shape is clear: when the dot energy enters the Fermi level gap, the current rises, and continues to flow throughout the region between the black lines. Once the dot energy is larger than the higher Fermi level, current stops flowing. This is because, when the dot energy is in between the Fermi energies, electrons can 'fall' from the higher (in Fermi energy) lead's states, down onto the dot, and further down into the other leads energy states. This current does not flow when the dot energy is above or below the Fermi levels.

The slight curvature at the Fermi levels is due to the non-zero temperatures. This is because, as is shown by the Fermi function, electrons can be in states above the Fermi level at finite temperatures. This allows higher energy electrons to transport across the dot before it enters the Fermi gap (bottom left corner smoothing), and just after it leaves (bottom right corner smoothing).

The suppression of current observed in the top left and right corners of the curve occurs due to the competing flow of electrons with energy just above the Fermi level from the opposite lead, due to its own finite temperature.

4.2 SATURATION CURRENT

From the graphs in Section 4.1 it can be seen that, although the current grows as the dot energy passes through the gap in the Fermi levels, it nonetheless peaks at a finite value.

The maximum possible current reached in this process is known as the saturation current, I_{sat}. The analytic expression for the saturation current can be derived by considering the behaviour of the model as the difference in the Fermi levels of the two leads tends to infinity.

Mathematically, $E_{FL} \to -\infty$, and $E_{FR} \to \infty$. Applying this to the standard definition of the Fermi functions (equation 2.14) leads to $f_L \to 0$ and $f_R \to 1$. In turn, this means the lesser self-energies for each lead become $\Sigma_L^< = 0$ and $\Sigma_R^< = i\Gamma_R$.

Applying these results to equation 3.11 and evaluating the expression in Mathematica, the saturation current is found to be:

$$I_{sat} = \frac{\Gamma_L \Gamma_R}{\bar{\Gamma}} \tag{4.1}$$

This makes intuitive sense as it takes the Fermi levels and temperatures, literally, out of the equation, only depending on the tunnelling rate energies across the lead-dot barriers.

This expression highlights the purpose of the Digamma function (and its argument) in equation 3.12 as containers of the mathematical information needed to describe how each lead couples to the dot. In short, the Digamma functions mathematically represent the lead-dot transitions.

The fact, then, that the tunnelling rate energies for both left and right leads appear in each Digamma function, implies the coupling of the dot to one lead is not independent of the other lead's physical properties. That is, changing the tunnelling rate energy of one lead will affect the physical properties of the other lead-dot transition. Thus, the lead-dot transitions are not totally physically independent, an interesting and slightly counter-intuitive result.

4.3 THERMORESISTANCE

Figure 4B below shows the same blue current curve as Figure 4A, along with two new curves, where the leads are set at higher temperatures. Specifically, the left and right leads have both been raised to the same temperature in each case.

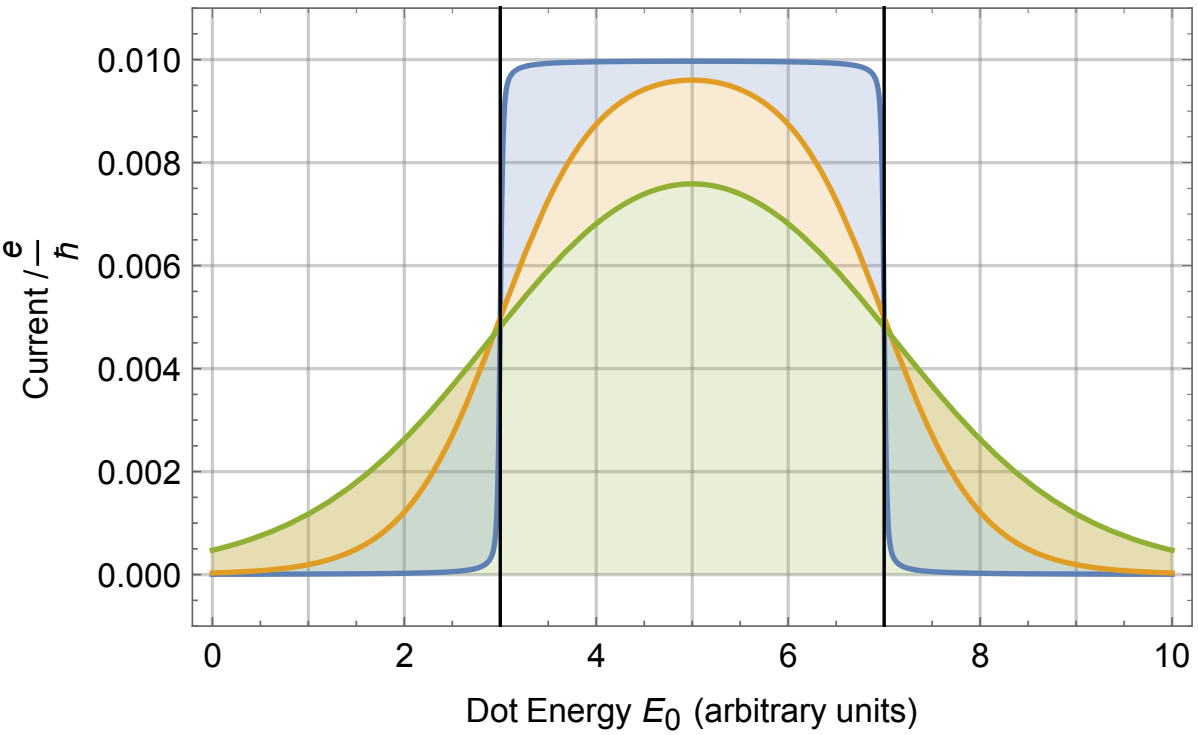

Figure 4B. A plot of current vs. dot energy in the lead-dot-lead model with both leads set jointly at three different temperatures. The blue curve represents a lower temperature of $k_B T_\alpha = 0.01$, and shows sharp transitions of current at the Fermi levels. The orange curve represents a warmer temperature of $k_B T_\alpha = 0.5$, showing smoother transitions with a slightly smaller peak current. The green curve represents the hottest temperature $k_B T_\alpha = 1$, causing the peak current to fall significantly. Higher temperatures resulting in lower currents is a sign of thermoresistance.

The orange curve shows that, when the temperature of the leads rises, the Fermi level transitions (where the dot energy passes the energy of the Fermi level) become increasingly undefined. This is as expected, as a temperature increase is simply a directionally random influx of kinetic energy.

The green curve shows more transition smoothing due to the higher temperature, while the peak current is now significantly lowered. This lower peak current is an indication of higher resistance at higher temperatures. Thus, the model is displaying signs of thermoresistance.

Lastly, it is noted that, for all three temperature settings, the current is equal when the dot energy is equal to a Fermi level. This is indicative of the Fermi level acting as a 'fulcrum' of the energy levels in the lead: the thermal energy injected into the system by higher temperatures equally distributes either side of the Fermi level. This means there is no directional bias added by thermal energy of any temperature when the dot energy is level with the Fermi energy.

4.4 THE THERMOELECTRIC EFFECT

With this lead-dot-lead model having finite temperatures for each lead as variables, it is possible to set up the system with different temperatures in each lead and a zero Fermi level gap. This gives a non-zero current, and is known as the thermoelectric effect. This is plotted in Figure 4C below:

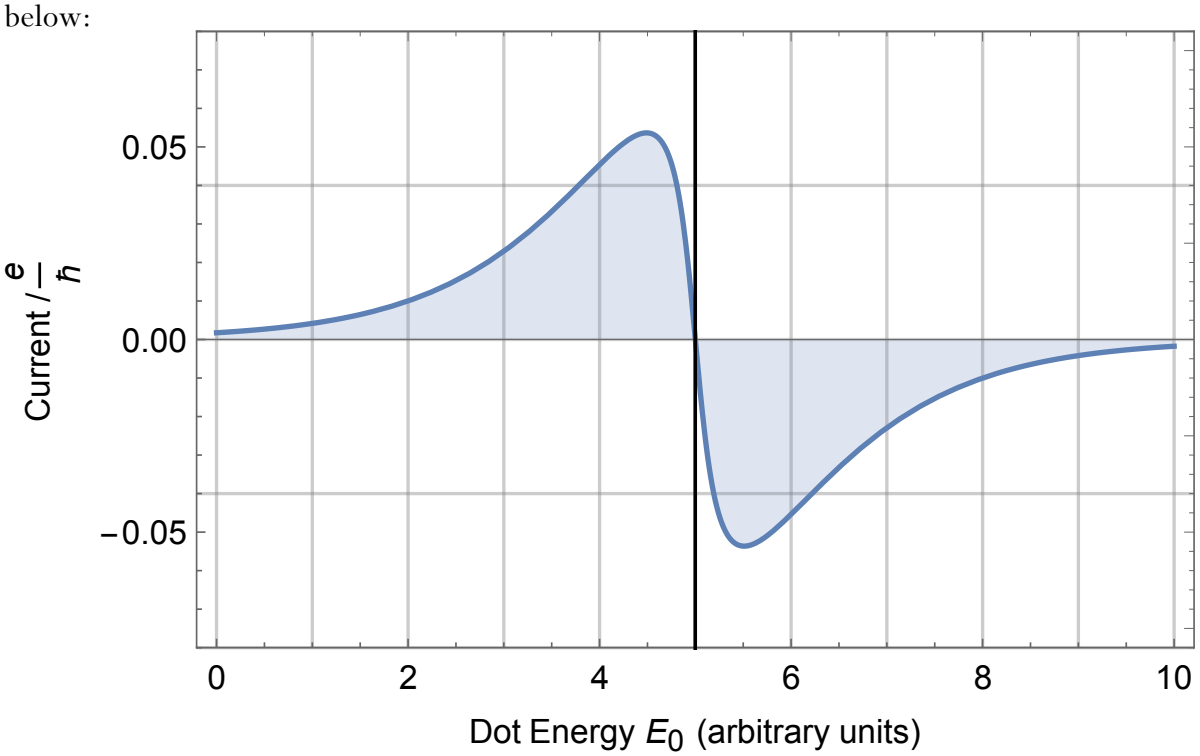

Figure 4C. A plot of current vs. dot energy in the lead-dot-lead model with the Fermi level gap set to zero and the lead temperatures set to $k_B T_R = 0.01$ and $k_B T_L = 1$. The tunnelling rate energies are set at $\Gamma_\alpha = 0.2$. The curve shows that the model exhibits the thermoelectric effect. The resultant current is antisymmetric about the joint Fermi level (black line), an indication the model captures the behaviour of electron holes as well as electrons.

The thermoelectric effect produces a current which is antisymmetric about the (joint) Fermi level. This is because, as the dot energy approaches the Fermi level, the energy of the electrons above the Fermi level in the lead with the higher temperature is sufficient for the electrons to 'fall' onto the dot and still transport across to the other lead.

As the dot energy approaches the Fermi level, this effect begins to occur in both directions, and thus the overall current reduces to zero.

Once the dot energy passes the Fermi level however, the same effect begins not with electrons, but with electron holes (empty electron energy states). This results in identical current but in the reverse direction, and is evidence of the model displaying the electron-hole symmetry of the system.

Lastly, the thermoelectric effect is shown in a system with a constant Fermi level gap (Figure 4D). The different curves show increasing temperature difference between the leads. The right lead temperature is set constant at $k_B T_R = 0.01$, whilst the left lead temperature is set at increasing values of $k_B T_L = 0.01, 0.25$ and 1 for the blue, orange and green curves respectively.

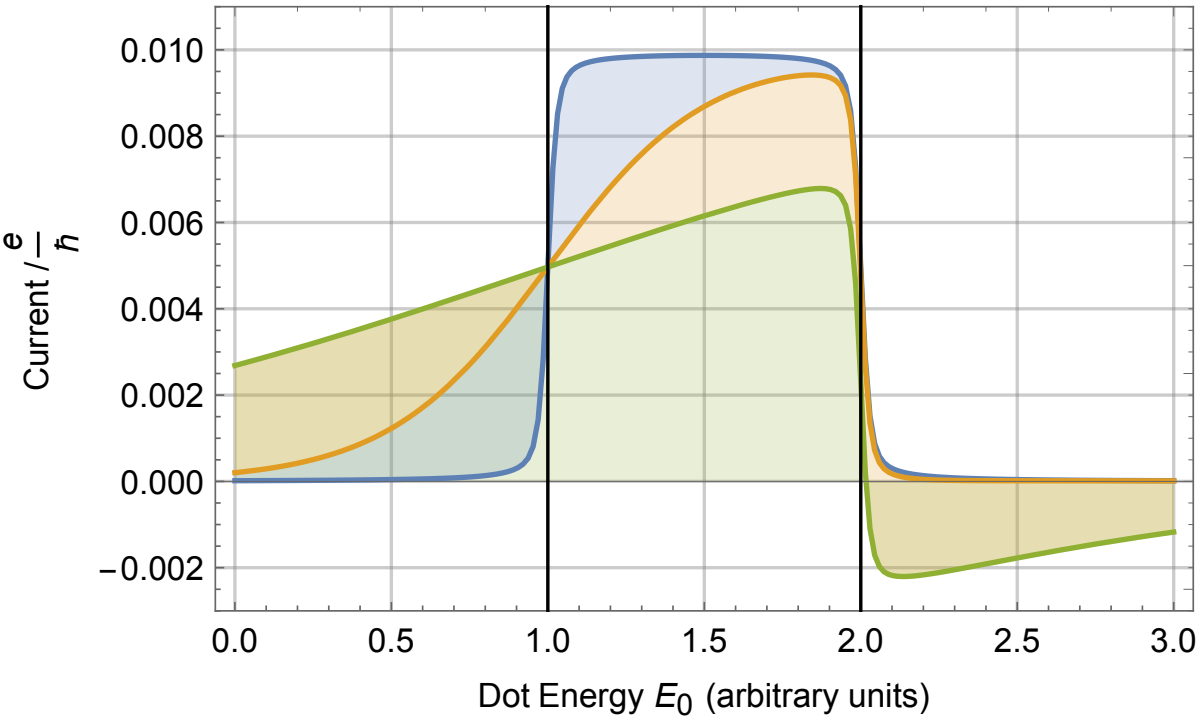

Figure 4D. A plot of current vs. dot energy showing the thermoelectric effect with the model set up with a constant Fermi level gap and increasing temperature differences in the leads ($k_B T_R = 0.01$ and $k_B T_L = 0.01, 0.25, 1$ for the blue, orange and green curves respectively). The thermal energy gap for the green curve is comparable in size to the Fermi energy gap. This means the reverse current flow of the thermoelectric effect becomes significant enough to change the direction of the overall current altogether as the dot energy rises above the higher Fermi level.

The interesting new feature of these curves comes in the bottom right of the green curve: the current is reversed! This is because, as the temperature difference increases and the thermal energy difference is of comparable size to the Fermi energy gap, there are electrons in the hotter left lead (which has a smaller Fermi level) which have enough energy to transport across the junction in the opposite direction. This reduces the current when the dot energy is between the Fermi levels. Once the dot energy is larger than the larger Fermi level, only this reverse current remains.

This can also be understood as the electron hole current becoming significant compared to, and eventually greater than, the electron current.

4.5 DENSITY ON THE DOT

By going through a similar process as in Section 3.2, the density on the dot (the energy integral of $G^<$) was derived and evaluated in Mathematica:

$$\rho = \frac{1}{2} - \frac{i}{\pi\bar{\Gamma}}\{\Gamma_L \cdot \Delta\psi(z_L) + \Gamma_R \cdot \Delta\psi(z_R)\} \tag{4.2}$$

The density is plotted as a function of the dot energy in the Figure 4E below. The model is set with a Fermi level gap, and with temperatures and tunnelling rate energies in each lead equal ($\Gamma_L = \Gamma_R$ and $T_L = T_R$).

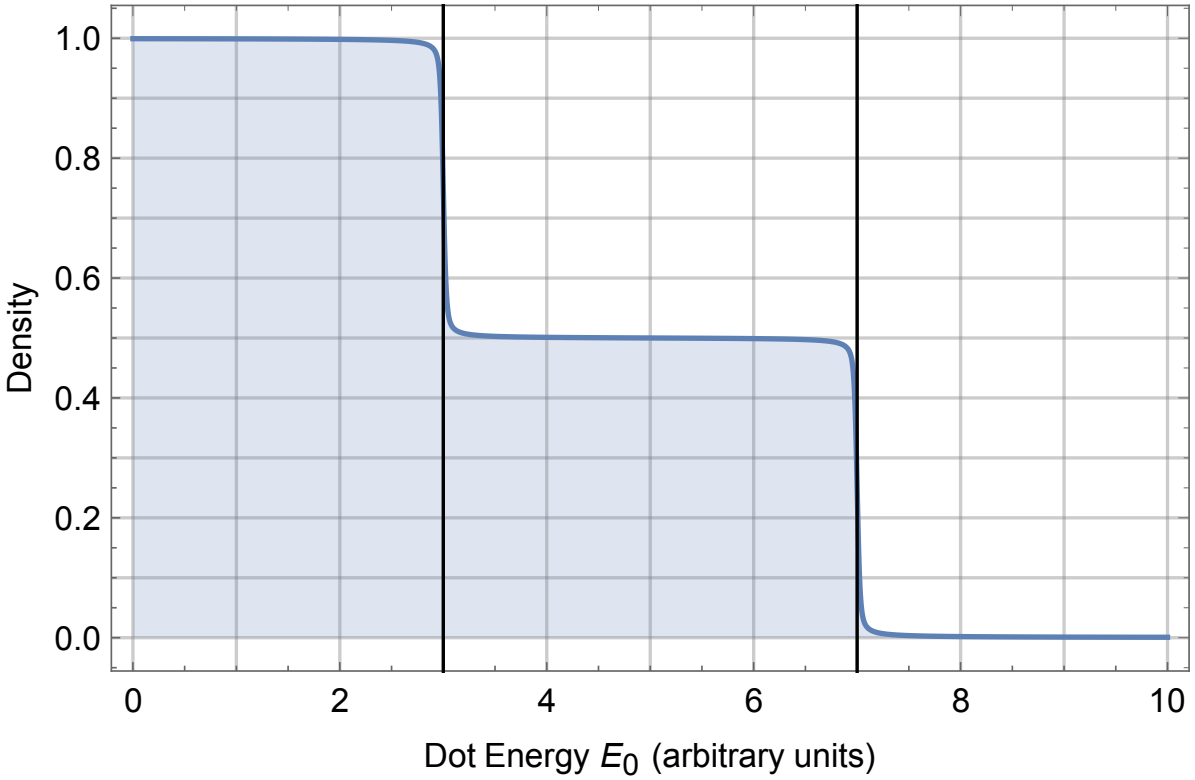

Figure 4E. A plot of density vs. dot energy. The likelihood of detecting the electron on the dot (the density on the dot) goes from a certainty ($\rho = 1$) when the dot energy is below the Fermi levels, to impossible ($\rho = 0$) when it is above. When in between the Fermi levels, $\rho = 0.5$, indicating it is equally likely to detect a filled electron state (an electron) or an empty electron state (an electron hole) on the dot.

The plot shows that, when the dot energy is below the Fermi level gap, the dot is 'full' of electrons ($\rho = 1$); and when it is above the gap, it is empty of electrons ($\rho = 0$). When the dot energy enters the region between the Fermi levels, the density goes to $\rho = 0.5$, indicating the dot is half 'full' of electrons. This can be interpreted as the dot being half occupied by electrons and half occupied by electron holes when current flows across the junction, and emphasises the time-averaged, steady-state nature of the model due to its basis in energy-dependent (not time-dependent) Green's functions.

Looking more closely at equation 4.2, it is seen that, unlike equation 3.12 for the current, the tunnelling rate energies appear asymmetrically to left-right exchange. This suggests that changing one should have a different effect to changing the other.

Figure 4F below shows the density on the dot of the system with the left and right tunnelling rate energies varied independently. The blue curve is as in Figure 4E, with the orange curve increasing the right lead's tunnelling, and the green curve increasing the left's.

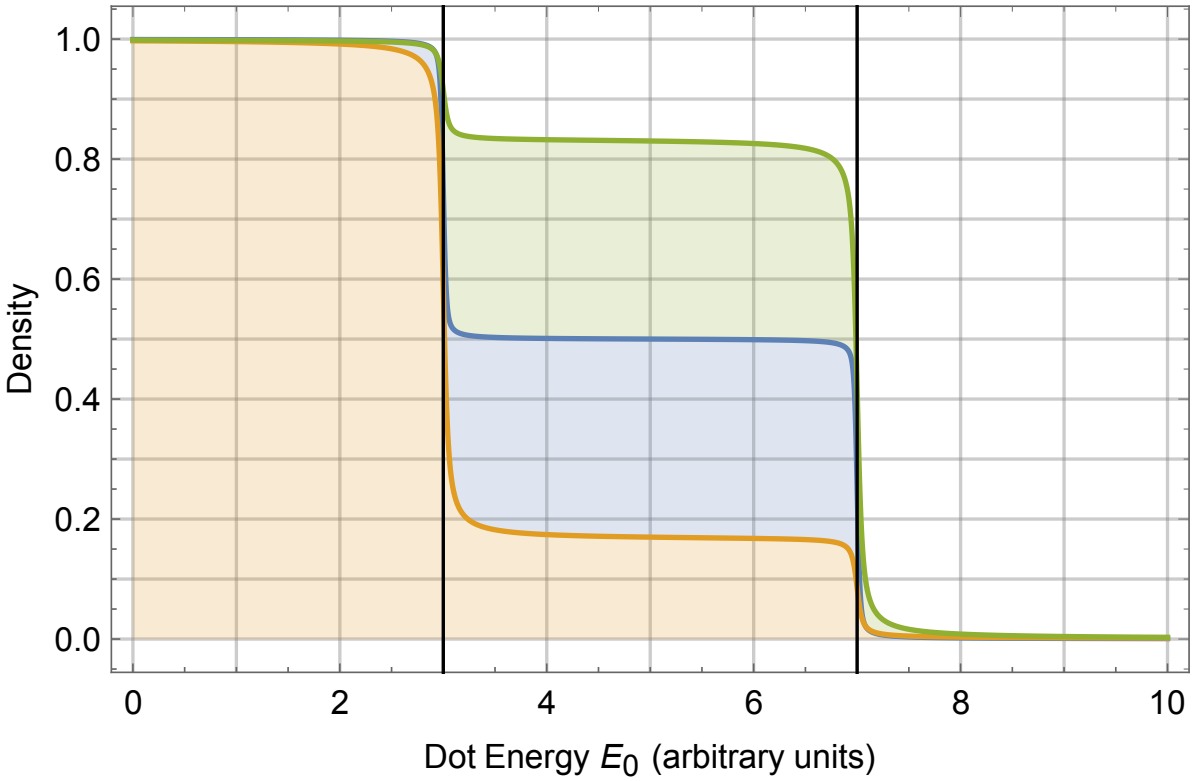

Figure 4F. A plot of density vs. dot energy with varied tunnelling rate energies and a constant Fermi level gap. The model is set up with $\Gamma_L = \Gamma_R$ (blue), $\Gamma_L > \Gamma_R$ (orange), $\Gamma_L < \Gamma_R$ (green). When tunnelling increases from the higher energy right lead, more electrons can flow onto the dot, increasing the density (green). Increasing the tunnelling from the lower energy left lead allows more holes to flow on the dot, decreasing the electron density (orange).

The green curve shows a smaller density on the dot when its energy is between the Fermi levels. This is because, when tunnelling is made energetically easier from the higher energy lead, the steady-state is for a higher likelihood of an electron being on the dot. The same argument applies to the orange curve for the lower energy lead, except for electron holes not electrons, meaning the electron density itself is lowered.

Thus, changing the left lead's tunnelling rate energy has a distinct and opposite effect to changing the right lead's, as suggested by the mathematical structure of equation 4.2.

5 ADDING THE QUANTUM HARMONIC OSCILLATOR (QHO)

5.1 THE QHO ENERGY

To turn the lead-dot-lead model into a fully-fledged model of a nanoelectromechanical system, an oscillator is coupled to the dot. As the model aims to work at the size and energy scales of quantum mechanics, the oscillator is taken to be a Quantum Harmonic Oscillator (QHO). QHO's, unlike classical oscillators, have discrete energy levels, labelled n, given by:

$$E_n = \left(n + \tfrac{1}{2}\right)\hbar\omega \tag{5.1}$$

where $\hbar$ is the reduced Planck's constant and ω is the natural frequency of the QHO.

To couple this QHO to the lead-dot-lead model established in Sections 2 and 3, firstly the QHO energy must be incorporated into the theoretical basis of the model. In practice, doing this results in the simple addition of the QHO energy to each of the other two energy levels in the model:

$$E_0 \to E_{0,n} = E_0 + \left(n + \tfrac{1}{2}\right)\hbar\omega \tag{5.2}$$

$$E_{F\alpha} \to E_{F\alpha,m} = E_{F\alpha} + \left(m + \tfrac{1}{2}\right)\hbar\omega \tag{5.3}$$

Here, the choice to give the QHO energies different labels, n and m, is made deliberately. This is because the interactions involved in the electrons going from dot to lead (or vice versa) affect the QHO, and hence can change its energy state. These interactions are between electrons in the lead-dot-lead system and phonons in the oscillator. The labels for the QHO energy levels can be read as labels for the initial and final QHO energy states.

The Fermi function transforms due to these energy substitutions, picking up an index denoting the oscillator energy level in the following way:

$$f_\alpha \to f_{\alpha,n} = \frac{1}{2} - \sum_{q=-\infty}^{\infty} \left\{ \frac{E - E_{F\alpha} - \left(n + \frac{1}{2}\right)\hbar\omega}{k_B T_\alpha} - i(2q+1)\pi \right\}^{-1} \tag{5.4}$$

5.2 THE S-MATRIX

The interaction of the electrons and phonons is modelled as a scattering process.

The core idea in formalising this scattering process mathematically is to consider the overlap of two wavefunctions: one for the dot in an unoccupied state (that is, no electron on the dot), and one for the dot in an occupied state.

This overlap is known as an S-matrix in quantum field theories [12]. The S-matrix is responsible for transforming between the occupied and unoccupied representations of the dot, and is necessary for considering the transport of electrons across the (now QHO-coupled) lead-dot-lead system.

Written $\Phi_{n,m}(x)$, the value of the S-matrix depends on how much the QHO is affected by the coupling to the electrons. The variable x is dimensionless and is defined by:

$$x = \frac{x_o}{l} \tag{5.5}$$

where x_0 is the shift in the amplitude of the QHO oscillations due to the coupling, and l is the zero-point amplitude of the QHO.[10] The variable x is interpreted as the amount, or strength, of the coupling.

The S-matrix describes how the energy required for the resonant tunnelling of the electrons across the lead-dot-lead system is affected by the displacement of the QHO, affecting how the electrons are transported and how current flows.

Thus, the S-matrix provides the theoretical structure to model the key feature of NEMS: the feedback interaction between the electrical component (the lead-dot-lead system) and the mechanical component (the QHO).

5.3 ADVANCED & RETARDED GREEN'S FUNCTIONS (WITH QHO)

To incorporate the coupling of the QHO into the Green's functions formalism used in Section 2, the scattering due to the S-matrix is treated in a way not too dissimilar to a perturbation. This is because there are again two Green's functions, 'unscattered' and 'scattered', similar to there being two Green's functions (unperturbed and perturbed) used in Section 2.

[10] For a QHO of mass m and natural frequency ω, the zero-point amplitude is $l = \sqrt{\frac{\hbar}{m\omega}}$. The shift on the oscillations of the QHO due to coupling in an electric field $\mathcal{E}$, is $x_o = \frac{e\mathcal{E}}{m\omega^2}$.

The unscattered Green's functions (advanced and retarded) are given as:

$$g_n^{a(r)} = \left(E - E_0 - \left(n + \frac{1}{2}\right)\hbar\omega - \Sigma_n^{a(r)}\right)^{-1} \tag{5.6}$$

These resemble the perturbed Green's functions from Section 2 because they still capture the lead-dot-lead coupling, except now with the QHO energy simply inserted as outlined in Section 5.1. Note that the self-energy term depends on the state of the oscillator. This is explained in Section 5.4.

The scattered advanced and retarded Green's functions are then defined by:

$$G_{nm}^{a(r)} = \sum_{n'} \Phi_{mn'}^* \, g_{n'}^{a(r)} \Phi_{mn'}^* \tag{5.7}$$

There are a few aspects to understand about equation 5.7. Firstly, the 'unperturbed' Green's functions ($g_{n'}^{a(r)}$) represent the dot in an occupied state, whilst the 'perturbed' Green's functions ($G_{nm}^{a(r)}$) represent the dot (and the phonons transferred in the scattering process) in an unoccupied state. With the state going from occupied to unoccupied due to the S-matrices, a basis is provided for propagation of states, and hence electron movement.

Secondly, the S-matrices serve the function of taking a phonon from an initial state n to a final state m. It is noted that the second S-matrix in equation 5.7 is the complex conjugate with its indices reversed, otherwise known as the Hermitian conjugate of the matrix. This is evidence of the S-matrix acting as a unitary operator, and indicates it is changing the representation of the system.

Thirdly, the sum over n' means that, to fully describe going from an occupied to unoccupied state, the energetic interactions of the initial and final states with all phonon states need to be accounted for.

5.4 THE QHO TEMPERATURE

In order to bring the entirety of the model into the finite temperature domain, the QHO can also be assigned a non-zero temperature. Recalling that the self-energy is defined as the exact contribution to the dot energy due to coupling with the leads, the coupling to the QHO at finite temperature affects this contribution. Specifically, the lesser self-energies for left and right leads become:

$$\Sigma_{\alpha,n}^{<} = i\Gamma_\alpha f_{\alpha,n} B_n \tag{5.8}$$

where B_n is a weighting factor determined by the statistical distribution of the energies of the phonons. This factor accounts for the availability of phonons in the different QHO energy levels through which conduction can occur.

For a QHO at temperature T_{QHO}, B_n is defined by:

$$B_n = e^{\frac{(n+\frac{1}{2})\hbar\omega}{k_B T_{QHO}}} \Big/ \sum_{n'} e^{\frac{(n'+\frac{1}{2})\hbar\omega}{k_B T_{QHO}}} \tag{5.9}$$

5.5 NON-EQUILIBRIUM GREEN'S FUNCTIONS WITH THE QHO

Recalling the form of equation 2.18, the non-equilibrium Green's function for the lead-dot-lead system coupled to a QHO is written:

$$G^<_{nn} = \sum_{n'} G^r_{nn'}\, \Sigma^<_{n'} G^a_{n'n} \tag{5.10}$$

In general, a matrix $G^<_{nm}$ can be written. Here, however, one of the indices can be dropped because the general lesser self-energy matrix $\Sigma^<_{nm}$ only has non-zero diagonal terms ($m = n$).[11]

5.6 THE CURRENT EQUATION WITH THE QHO

Applying the Green's functions in the same way as in Section 2, the expression for the current from each lead (in the QHO-coupled) system can be reached:

$$I_\alpha = \frac{1}{2\pi} \sum_n \int_{-\infty}^{\infty} \Sigma^<_{\alpha n}(G^r_{nn} - G^a_{nn}) + G^<_{nn}(\Sigma^a_{\alpha n} - \Sigma^r_{\alpha n}) dE \tag{5.11}$$

Again, taking $I = I_L - I_R$, the current equation is then:

$$I = \frac{1}{2\pi} \int_{-\infty}^{\infty} (\Sigma^<_{Ln} - \Sigma^<_{Rn})(G^r_{nn} - G^a_{nn}) dE - (\Gamma_L - \Gamma_R)\rho_{nn} \tag{5.12}$$

Where the density matrix, now coupled to the QHO, is defined by:

$$\rho_{nm} = \frac{1}{2\pi i} \int_{-\infty}^{\infty} G^<_{nm}\, dE \tag{5.13}$$

[11] $\Sigma^<_{nm}$ is a diagonal matrix because it is defined as purely the interaction between the dot and the lead. If it had non-zero off-diagonal elements, this would contain information about the phonon energy changing, which is an interaction with the QHO.

6 RESULTS (WITH QHO)

6.1 SOLVING THE CURRENT EQUATION (WITH QHO)

To model the lead-dot-lead system coupled to the QHO, the equation 5.12 needs to be solved. Taking the tunnelling rates to be symmetric (that is, $\Gamma_L = \Gamma_R = \Gamma$), simplifies equation 5.12, and allows the following form to be derived:

$$I = \frac{1}{2\pi} \sum_{n,m} B_n \, |\Phi_{nm}|^2 \cdot i\Gamma \cdot \{\Delta\psi(z_{Lnm}) - \Delta\psi(z_{Rnm})\} \tag{6.1}$$

where the arguments for the Digamma functions now incorporate the initial and final QHO states:

$$z_{\alpha nm} = \frac{1}{2} + \frac{\bar{\Gamma} + i(\{E_{F\alpha} + (n + \frac{1}{2})\hbar\omega\} - \{E_0 + (m + \frac{1}{2})\hbar\omega\})}{2\pi k_B T_\alpha} \tag{6.2}$$

6.2 NUMERICAL LIMITATIONS

The equation for QHO-coupled current contains a sum over all initial and final phonon states. As a QHO has infinite energy levels, to compute the current analytically requires a sum over an infinite number of states. For the computational method used in this project, this sum would take infinite time to compute. Thus, the compromise was made to only sum over the lowest ten states of the QHO.

The second alteration needed to numerically compute the current was in the S-matrix. The use of the S-matrix and its Hermitian conjugate relies on their unitary property: that is, their matrix product equals the identity matrix. This relies on all the states being present in the matrix, which isn't the case for a finite-state, numerically computed model. Therefore, to preserve the unitarity of the compromised S-matrix, the inverse is used instead of the Hermitian conjugate.

6.3 CURRENT VS. DOT ENERGY (WITH QHO)

To current for the QHO-coupled system (with the QHO temperature low) is plotted in figure 6A below.[12]

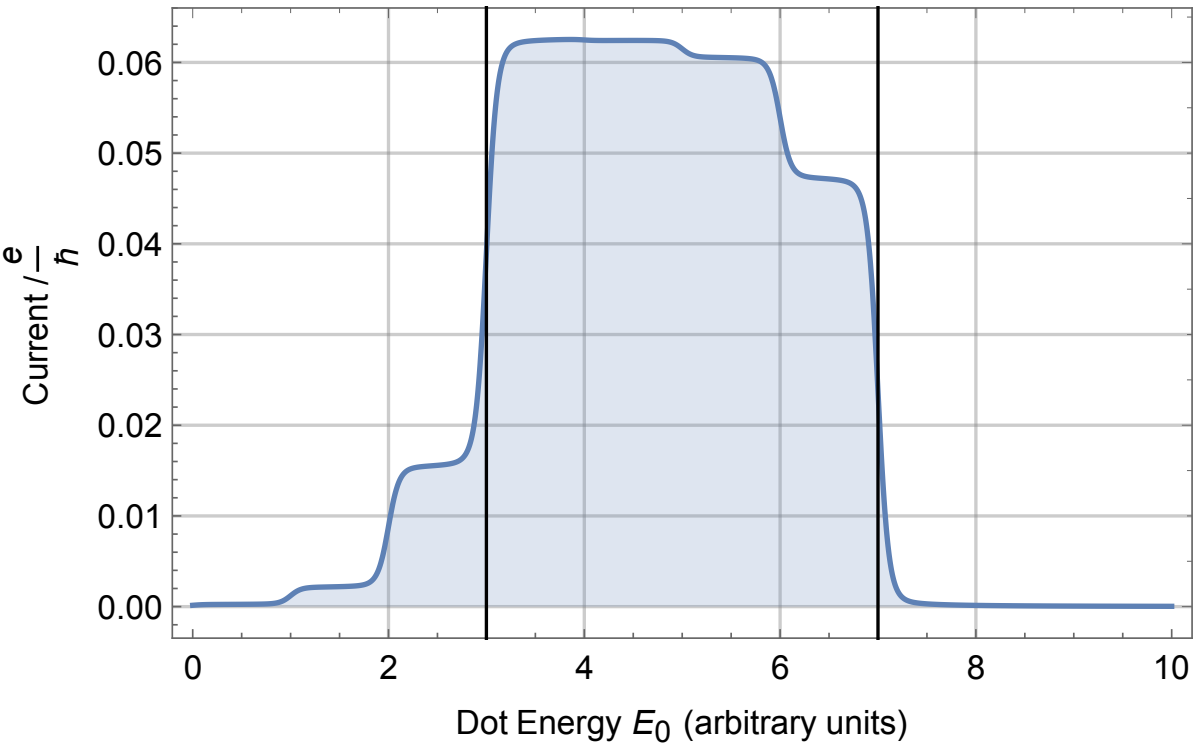

Figure 6A. A plot of the current vs. dot energy for the lead-dot-lead system coupled to a QHO at low temperature ($k_B T_{QHO} = 0.01$). The extra steps increasing and decreasing the current are due to the new energy routes made available by phonon creation on the QHO. Phonons are created before the dot enters (exits) the Fermi level gap, allowing electrons (holes) to flow onto and across the dot, increasing (decreasing) the current.

The form is similar to the current curves in Section 4, except there are added steps increasing the current before the dot energy enters the Fermi level gap, and steps decreasing the current after it leaves. These steps can be explained by the QHO-coupling allowing for phonon creation, and are indicative of the quantum 'ladder' of the QHO energy levels.

Phonon creation is a transfer of energy from the electron states in the lead to the oscillator states coupled to the dot. Thus, having the QHO coupled to the system introduces new energy 'routes' to transport electrons (in the case of increased current bumps) and holes (in the case of decreased current bumps) onto and off the dot, creating phonons.

[12] The oscillator energy scale is set to $\hbar\omega = 1$ (in arbitrary units) for all figures in this section.

The current for the QHO-coupled system for an increased QHO temperature is plotted in Figure 6B below.

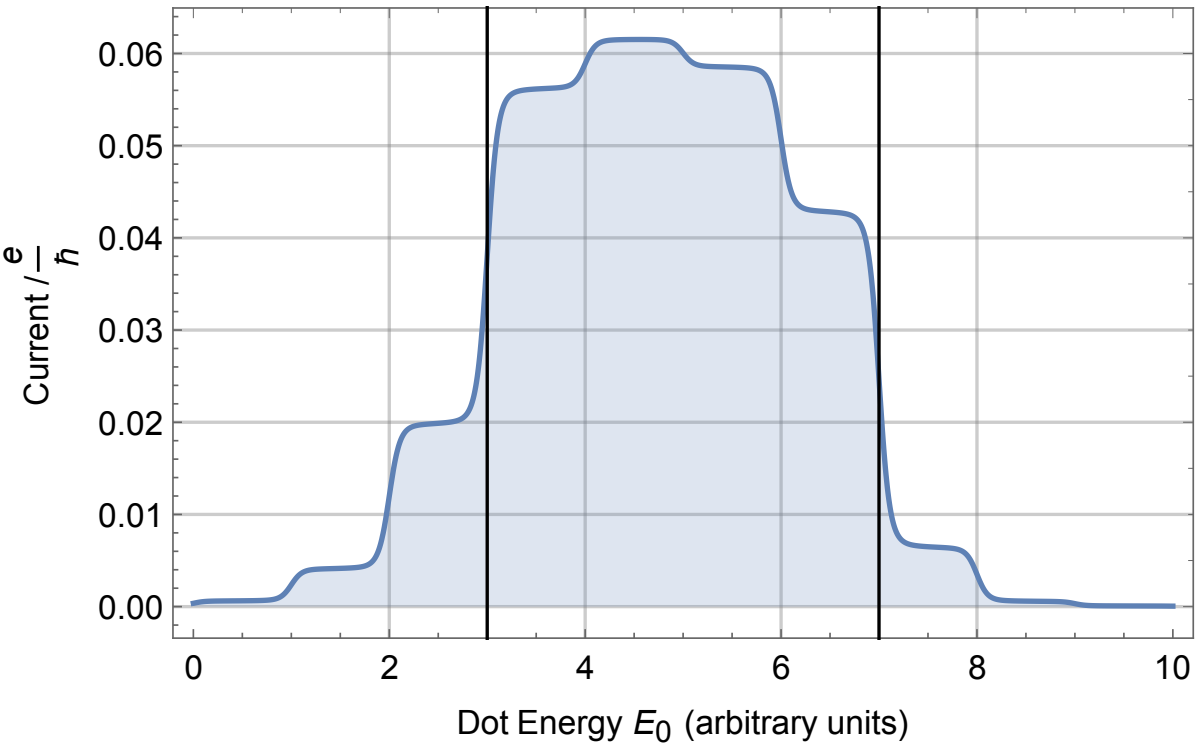

Figure 6B. A plot of the current vs. dot energy for the lead-dot-lead system coupled to a QHO at a high temperature ($k_B T_{QHO} = 1$). The steps increasing and decreasing the current around the Fermi level transitions are due to the new energy routes made available by phonon creation and (due to the larger temperature) annihilation on the QHO.

This figure shows a similar curve to Figure 6A, except now with extra steps reducing the current just after the dot energy enters the Fermi level gap, and increasing the current just as it leaves.

These steps can be explained by phonon annihilation. By giving the QHO a higher temperature, more higher energy phonon states are filled (according to the Boltzmann factor). Phonon annihilation transfers energy off the dot and into the leads. This allows for holes to be created and to flow onto the dot and across the junction as the dot energy first enters the Fermi level gap, lowering the current. By electron-hole symmetry, the phonon annihilation also allows electrons to flow across the junction once the dot energy exits the Fermi level gap, thus raising the current.

6.4 SATURATION CURRENT (WITH QHO)

Going through the same process as in Section 4.2 the saturation current for the QHO-coupled system can be derived. The result is:

$$I_{sat} = \Gamma \sum_{n,m} B_n \, |\Phi_{nm}|^2 \tag{6.3}$$

This is the same result as in Section 4.2, except with an added factor due to the QHO coupling, which increases the saturation current.

Assuming the saturation current cannot be infinite suggests that the sum over QHO states converges, despite still being assumed to have infinite terms in the derivation. This suggests the summation terms could be mathematically manipulated such that the infinite sum converges, allowing the numerical limitation to be lifted.

6.5 THE THERMOELECTRIC EFFECT (WITH QHO)

Figure 6C below plots the current due to the thermoelectric effect in the QHO-coupled model with the Fermi levels set equal.

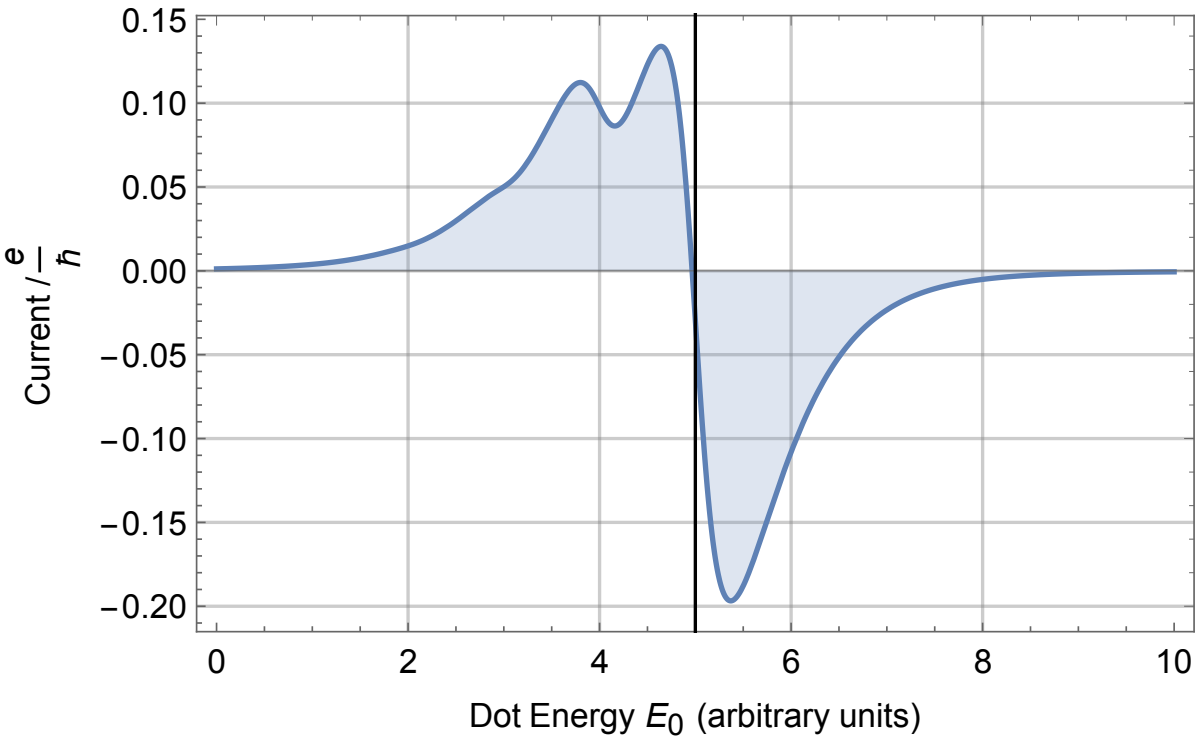

Figure 6C. A plot of the current vs. dot energy due to the thermoelectric effect for the QHO-coupled system with the Fermi levels equal ($k_B T_{QHO} = 0.05, k_B T_L = 0.05, k_B T_R = 0.5$). The bumps in the current are due to phonon creations introduced by the QHO which result in holes being created and flowing across the junction, reducing the electron current as the dot energy approaches the Fermi level.

The curve retains the antisymmetric shape present in the no-QHO case, except with bumps reducing the current as the dot energy approaches the joint Fermi level.

The presence of these bumps below the Fermi level but not above it emphasises that the cause is phonon creation (not annihilation). This is because phonon creation requires the annihilation of an electron (the creation of an electron hole), reducing the electron current. To reduce the absolute value of the current once the dot energy is above the Fermi level, phonon annihilation needs to occur to create electrons to oppose the hole current.

Figure 6D below plots the same setup as Figure 6C, except the QHO temperature is raised. This results in extra bumps increasing the current when the dot energy is above the Fermi levels.

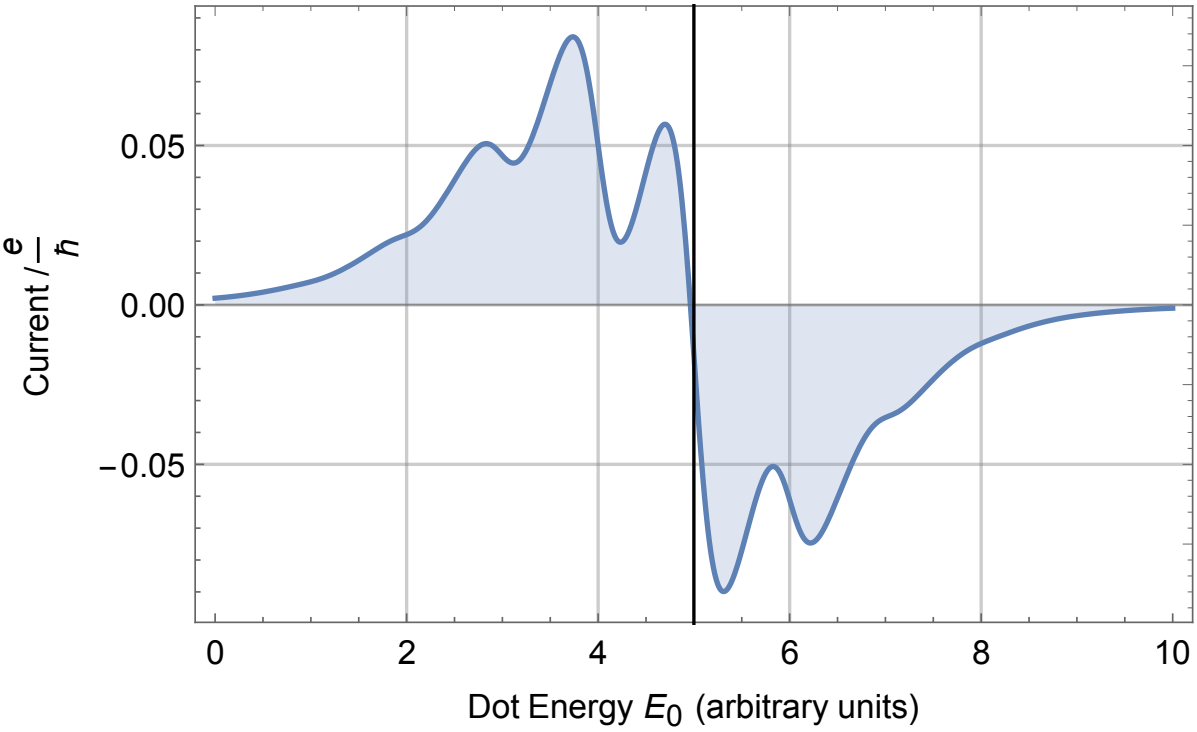

Figure 6D. A plot of the current vs. dot energy due to the thermoelectric effect for the QHO-coupled system with the Fermi levels equal and the QHO at a higher temperature ($k_BT_{QHO} = 2, k_BT_L = 0.05, k_BT_R = 0.5$) The bumps decreasing (increasing) the current before (after) the dot energy passes the Fermi level are due to phonon creations (annihilations) introduced by the QHO which result in holes (electrons) being created and flowing across the junction.

The extra bumps appear because a higher QHO temperature means more phonons are in higher energy states. This results in the increase in phonon annihilations (and electron creations), increasing the current (and reducing the reverse hole current).

Also, by introducing phonon annihilations, the antisymmetric nature of the current due to the thermoelectric effect is restored. This is due to the returning symmetry of electron and hole currents when both creation and annihilation of phonons is occurring at comparable rates.

6.6 DENSITY MATRIX, ENTANGLEMENT & ENTROPY

One question of interest is whether there is any evidence of quantum entanglement in this model of a lead-dot-lead junction coupled to a QHO. Quantum entanglement is defined between two particles as when the quantum state of one particle cannot be defined without the quantum state of another. [13]

The density matrix ρ_{nm} of the model contains information on the occupation of different phonon energy states of the system. By diagonalising the matrix, the eigenvalues and eigenvectors can be obtained, labelled by oscillator states.

The eigenvalues give the occupation probability of an electron being detected in the labelled state. These probabilities are conditional on the electron being in an oscillator state to begin with, so they sum to 1.

The eigenvectors contain the values of interest for entanglement. The n^{th} 'coordinate' of the m^{th} eigenvector gives the coefficient of n^{th} initial oscillator state needed to define an electron in the m^{th} final state.

If there is no entanglement then only the m^{th} coordinate of the m^{th} eigenvector would be non-zero, as it does not need to be defined by a superposition of any other states. Thus, in a matrix composed of the eigenvectors, the presence of non-zero off-diagonal elements is a sign of entanglement.

To get a measure of the entanglement, the von Neumman entropy was considered, defined by:

$$S = -Tr(\rho \ln \rho) \tag{6.4}$$

This measure of entanglement generalises the definition of the Gibbs entropy from thermodynamics to quantum mechanics, and can also be interpreted as a generalisation of the Shannon entropy from information theory. [14]

Using equation 5.13, an expression for the density matrix was derived and computed in Mathematica. The von Neumann entropy was then calculated for 5×5 matrices with the model set with increasing QHO-coupling strength. The results are plotted in Figure 6E.

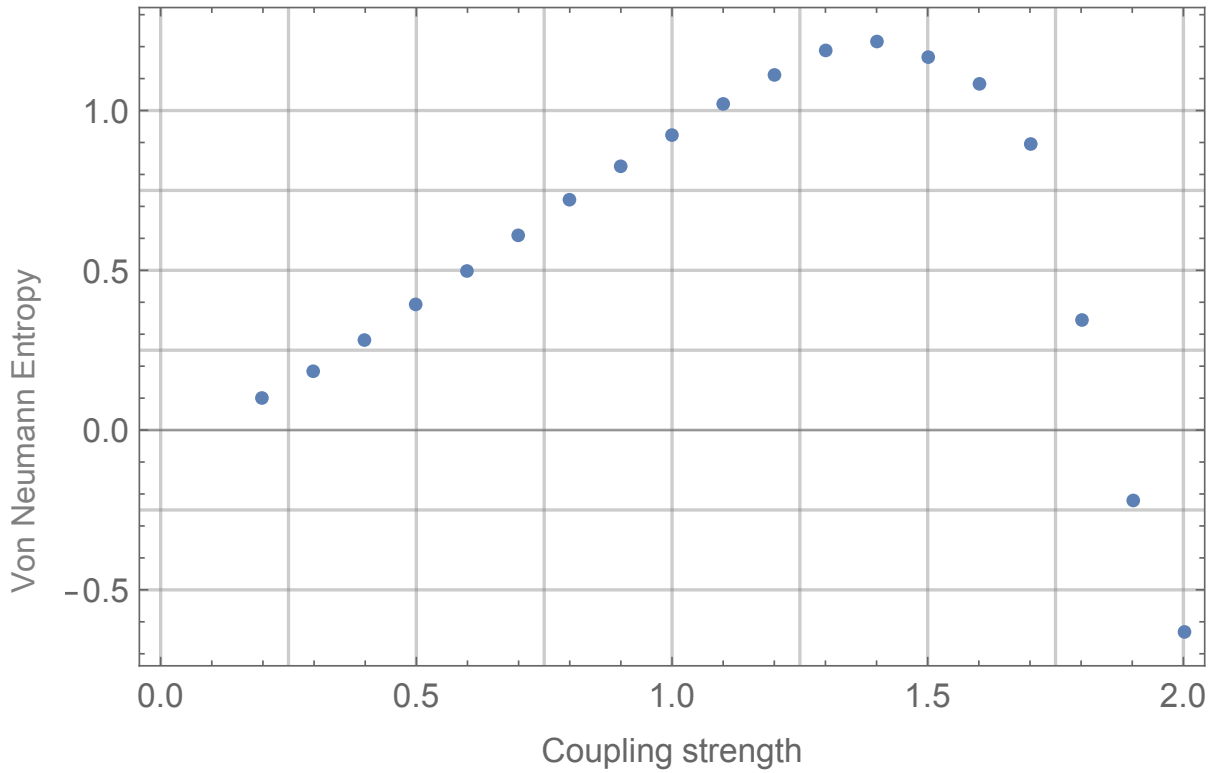

Figure 6E. A plot of the von Neumann entropy vs. the coupling strength of the QHO to the lead-dot-lead system. The linear relationship up to a coupling strength of 1.4 *shows how the system increases its level of entanglement the more strongly the QHO is coupled, an intuitive result. The rapid drop-off into negative, unphysical values at higher coupling strengths suggests a non-linear response is not being accounted for.*

Figure 6E shows the entanglement growing linearly with coupling strength up to a peak value of 1.22 at $x = 1.4$. This linear response shows the model is behaving physically sensibly for weaker QHO couplings.

After this peak however, the values begin to fall at a faster rate, ultimately into negative, unphysical values for the von Neumann entropy. This is a sign of the system responding non-linearly to stronger QHO couplings, something the model is evidently not well-equipped for.

It is interesting to note that the peak entropy possible for any system is given by the natural logarithm of the number of states, in this case $\ln 5 = 1.61$. This suggests the entropy might yet have kept increasing before non-linear effects kicked in.

The form of this graph also highlights how the S-matrix, which is changed by the increased coupling strength, is responsible for entangling the states.

7 CONCLUSIONS

7.1 ACHIEVEMENTS

In conclusion, the quantum transport in a model of nanoelectromechanical systems was studied by investigating the electron current in a lead-dot-lead system, firstly without, and then with, coupling to a QHO.

The use of the Matsubara sum allowed for the derivation of the behaviour of the system at non-zero temperatures, which is the main achievement of novel work in this project, built upon the work in Muhammad Tahir's PhD.

The simple lead-dot-lead model behaved in a physically sensible way, producing current when the dot energy was between the two Fermi levels, with smoothing at the transitions modulated by the finite lead temperatures. The novel effect of current due to the thermoelectric effect was shown capable of reversing the current flow; and the density on the dot was investigated for its behaviour as the tunnelling rate energy in each lead varied.

The QHO was then coupled to the lead-dot-lead system. Investigating the current for this coupled system, the presence of phonon creation and annihilation was detected, highlighting the fundamental electron-hole symmetry present in the system. Detecting annihilation was a novel result, as this required the incorporation of a finite QHO temperature. Next, the density matrix was investigated, which showed the model to exhibit quantum entanglement of the different energy states, which increased as the QHO-coupling increased.

Thus, in identifying the various phenomena and explaining their physical origins, a deeper understanding of NEMS was attained, achieving the main aim of the project.

7.2 FUTURE EXPLORATIONS

The main opportunity for future exploration lies in investigating the entanglement present in the QHO-coupled system. Understanding this better could expose new ways to manipulate electrons and phonons in NEMS, perhaps leading to new techniques for, say, information storage, cooling, or force detection.

Other avenues of future work include: studying the conductance and resistance of the lead-dot-lead junction, perhaps in relation to the thermoresistance observed; investigating whether a 'gamma current' exists for the QHO-coupled system; or considering whether the infinite sums encountered in coupling the QHO can be written in a form that converges: a more mathematically pure investigation.

8 BIBLIOGRAPHY

8.1 CITATIONS

[1] M. Roukes, "Nanoelectromechanical systems face the future," Physics World, pp. p25-31, February 2001.

[2] "Nanoelectromechanical systems," [Online]. Available: https://en.wikipedia.org/wiki/Nanoelectromechanical_systems. [Accessed April 2017].

[3] A. Cho, "Researchers Race to Put the Quantum Into Mechanics," Science, vol. 299, pp. p36-37, 3rd January 2003.

[4] S. Shreshtha and S. Ranjit, "Suspended graphene applications in NEMS and MEMS," in 2016 13th International Conference on Electrical Engineering/Electronics, Computer, Telecommunications and Information Technology (ECTI-CON) , 2016.

[5] M. P. Blencowe, "Nanoelectromechanical systems," Contemporary Physics, vol. 46, no. 4, pp. p249-264, July-August 2005.

[6] M. Tahir, Quantum Behaviour in Nano-Mechanical Systems, PhD Thesis: Imperial College London, Condensed Matter Theory Group, 2010.

[7] "Matsubara frequency," [Online]. Available: https://en.wikipedia.org/wiki/Matsubara_frequency. [Accessed April 2017].

[8] J. Maciejko, "An Introduction to Nonequilibrium Many-Body Theory," in Nonequilibrium Perturbation Theory, Springer, 2007.

[9] A. Kamenev, "Introduction to Keldysh Formalism," The Capri Spring School on Transport in Nanostructures.

[10] J. Keller and M. Jarrell, "Lecture 5: The Non-Equilibrium Green Function Method," Louisiana State University: Department of Physics & Astronomy.

[11] C. R. Nave, "The Fermi-Dirac Distribution," Department of Physics and Astronomy, 2012. [Online]. Available: http://hyperphysics.phy-astr.gsu.edu/hbase/quantum/disfd.html. [Accessed April 2017].

[12] T. Lancaster and S. J. Blundell, Quantum Field Theory for the Gifted Amateur, Oxford: Oxford University Press, 2015.

[13] "Quantum entanglement," [Online]. Available: https://en.wikipedia.org/wiki/Quantum_entanglement. [Accessed April 2017].

[14] "Von Neumann entropy," [Online]. Available: https://en.wikipedia.org/wiki/Von_Neumann_entropy. [Accessed April 2017].

8.2 OTHER REFERENCES

M. Blencowe, "Nanomechanical Quantum Limits," Science, vol. 304, pp. p56-57, 2nd April 2004.

M. Blencowe, "Quantum electromechanical systems," Physics Reports, vol. 395, no. 3, pp. p159-222, May 2004.

M. D. LaHaye, O. Buu, B. Camarota and K. Schwab, "Approaching the Quantum Limit of a Nanomechanical Resonator," Science, vol. 304, pp. p74-77, 2nd April 2004.

A. D. O'Connell, M. Hofheinz, M. Ansmann, R. C. Bialczak, M. Lenander, E. Lucero, M. Neeley, D. Sank, H. Wang, M. Weides, J. Wenner, J. M. Martinis and A. N. Cleland, "Quantum ground state and single-phonon control of a mechanical resonator," Nature, vol. 464, pp. p697-703, 1 April 2010.

H. Haug and A.-P. Jauho, "Quantum Kinetics in Transport and Optics of Semi-conductors," in Equilibrium Green Function Theory, Springer, pp. 49-55.

M. Pourfath, "Numerical Study of Quantum Transport in Carbon Nantube Based Transistors," July 2007. [Online]. Available: http://www.iue.tuwien.ac.at/phd/pourfath/diss.html. [Accessed April 2017].

"Density Matrix," [Online]. Available: https://en.wikipedia.org/wiki/Density_matrix. [Accessed April 2017].

D. W. Utami, H.-S. Goan and G. J. Milburn, "Charge transport in a quantum electromechanical system," Phys. Rev. B, 4th June 2004.

P. E. Blöchl, T. Pruschke and M. Potthoff, "Density-Matrix functionals from Green's functions," Phys. Rev. B, vol. 88, 21st November 2013.

M. B. Plenio and S. Virmani, "An introduction to entanglement measures," Quantum Information and Computation, 6th June 2006.

A. D. Armour and A. MacKinnon, "Transport via a quantum shuttle," Phys. Rev. B, vol. 66, 31st July 2002.

Y. Li, M. B. A. Jalil and S. G. Tan, "Nonequilibrium Keldysh Formalism for Interacting Leads -- Application to Quantum Dot Transport Driven by Spin Bias," Annals of Physics, vol. 327, 19th March 2012.

Utami, H.-S. Goan, C. A. Holmes and G. J. Milburn, "Quantum Noise in romechanical Shuttle," Phys. Rev. B, vol. 74, 28th September 2005.

D. Vasileska, D. Mamaluy, I. Knezevic, H. Khan and S. M. Goodnick, "Quantum Transport in Nanoscale Devices".

J. K. Sowa, J. A. Mol, G. A. D. Briggs and E. M. Gauger, "Vibrational effects in charge transport through a molecular double quantum dot," Phys. Rev. B, vol. 95, 17th February 2017.

D. A. Ryndyk, "Theory of Quantum Transport at the Nanoscale: An Introduction," Springer, 2016.